Simulating the modulation response of VCSELs: the effects of diffusion capacitance and spatial hole-burning

Y. Liu, W.-C. Ng, F. Oyafuso, B. Klein and K. Hess

Abstract: The comprehensive semiconductor laser simulator, Minilase, has been extended to simulate the dynamic response of vertical cavity surface emitting lasers (VCSELs). Unlike conventional rate equation approaches, Minilase is capable of correctly modelling nonlinear gain effects in the modulation response without the introduction of an empirical gain suppression factor. Various oxide-confined single-mode VCSEL structures are simulated with Minilase to examine the effects of real-space carrier transport on the modulation response in both vertical and lateral directions. It is demonstrated that a roll-off in the dynamic response is closely associated with the diffusion capacitance caused by vertical carrier leakage. By either grading the separate confinement regions or reducing the thickness of the SCH cavity, the vertical carrier leakage is shown to be greatly suppressed, and the modulation response is significantly improved. Simulations also reveal that the nonuniform HE11-like transverse optical intensity in the quantum well results in an overdamping of the relaxation oscillation, and this effect is greatly reduced by making the electrical aperture smaller than the optical aperture. Finally, a comparison with experimental results is presented and discussed.

1 Introduction

High-speed performance of vertical cavity surface emitting lasers (VCSELs) has become a key issue in short-range optical communications utilising VCSELs. Numerical simulations of the modulation responses of VCSELs are therefore important for both theoretical understanding and device optimisation. Great improvements in the steady-state and dynamic performances of VCSELs have been achieved through the development of selective oxidation of AlGaAs to confine both current injection and lateral optical field [1–3]. The complexity of such structures presents a challenge to device simulation for the following reasons. First, the introduction of oxide layers complicates the simulation of electrical properties due to the necessity to consider (at least) two dimensions in order to satisfy the boundary conditions of the electrical current and the electrostatic potential. Second, the optical properties require simulation in three dimensions with complex dielectric functions and open cavity boundary conditions. Third, simulation of the modulation response necessitates the inclusion of the additional dimension of time, and hence presents problems even for the largest available computational resources.

The commonly used approach to simulating laser diodes is based on a set of simple rate equations, as elaborated in many textbooks [4, 5]. This approach is numerically less demanding but cannot do justice to the requirements of simulating the modulation response because it can include nonlinear gain only in a phenomenological way. In fact, the modulation response computed by the rate equation approach overshoots the experimentally measured data significantly if one does not include an empirical gain suppression factor ε. Various attempts have recently been made to simulate the dynamic responses of index-guided VCSELs by using extended rate equation models [6, 7]. These models have taken into account vertical carrier transport, spatial hole-burning (SHB) and self-heating in a phenomenological way. However, the details of VCSEL structures, such as the thickness of cavities, the grading profile of separate confinement heterojunctions (SCHs) and the size of oxide apertures, can have a great influence on the modulation response. These effects cannot be accounted for by rate equation models and, as a result, predictions based on those models are incomplete.

Minilase is a comprehensive laser diode simulator based on basic diode physics and has demonstrated the capability to provide predictive and accurate simulations for edge-emitting lasers [8]. Recently, Minilase has been extended to simulate the fully coupled electrical and optical systems in VCSELs and some preliminary results have been presented [9]. To make the computation volume manageable, this simulator assumes axial symmetry in cylindrical co-ordinates, and thus simplifies the three-dimensional problem to a quasi three-dimensional one. With its

IEE Proceedings online no. 20020544

DOI: 10.1049/ip-opt:20020544

Paper first received 18th December 2001 and in revised form 22nd May 2002

Y. Liu, W.-C. Ng, and K. Hess are with the Beckman Institute, University of Illinois at Urbana-Champaign, 405 N. Mathews Ave., Urbana, IL 61801, USA

F. Oyafuso was with the Beckman Institute, University of Illinois at Urbana-Champaign and is now with Jet Propulsion Laboratory, 4800 Oak Grove Dr. MS 169-315, Pasadena, CA 91109, USA

B. Klein was with the Beckman Institute, University of Illinois at Urbana-Champaign and is now with National Institute of Standards and Technology—815.04, 325 Broadway, Boulder, CO 80305, USA

detailed treatment of carrier transport, Minilase contains enough fundamental physics to accurately model nonlinear gain suppression effects in the modulation response of VCSELs. In this paper, we focus on simulating the modulation response of VCSELs using Minilase, with the objective of studying the nonlinear gain effects due to carrier transport in both vertical and lateral directions. Heating of the carrier gas and the lattice is not included and only single-mode operation is considered. It is demonstrated that the vertical carrier leakage results in a diffusion capacitance, thereby causing a reduction in the modulation bandwidth. This effect is shown to be very sensitive to device structure. By either reducing the SCH cavity thickness or grading the SCH regions, the diffusion capacitance can be significantly suppressed, yielding a greatly improved bandwidth. In the transverse direction, effects due to lateral carrier diffusion and nonuniform transverse optical field are investigated. It is shown that the nonuniform transverse mode leads to overdamping of the relaxation oscillation. Huge improvements in the modulation response can be further achieved by making the electrical aperture smaller than the optical aperture.

2 The Minilase simulator for VCSELs

In Minilase, the problem of simulating VCSELs is divided into two well-defined parts: the electronic part and the optical part. Carrier transport in both real space and energy space is simulated in the electronic part while the optical intensity pattern, resonant frequency and optical loss rate are computed in the optical part. For devices with significant gain-guiding, the imaginary part of the refractive index in the quantum well (QW) region is also passed from the electronic solver to the optical solver, and Minilase iterates between the two parts until self-consistency is achieved. In this paper, we deal mainly with strongly index-guided structures and gain-guiding is negligible. Therefore, it suffices to treat the fundamental mode pattern as independent of the gain in the QW region.

Two optical solvers have been developed to solve the optical problem for oxide-confined VCSEL structures, one is based on a Green's function method and the other on a scalar effective index method. In both solvers, the entire device structure including the top and bottom DBR stacks are considered. In the Green's function approach, an integral eigenvalue equation for the modes is derived by requiring that the modes be self-supporting at threshold [10]. The oxide and gain regions are discretised and treated as distributed sources. Together with the dyadic Green's function operator for homogeneous multilayers and the method of moments, the homogeneous equation is transformed into a generalised eigenvalue problem. This allows the generalised eigenvalue problem to be solved at a few frequencies, ω, and thereby the resonant frequencies and threshold modal gain to be computed. However, as the volume of the discretised regions increases, the computation demands can become prohibitively large.

The scalar effective index method assumes a separable scalar field, $\phi(x, y, z) = \phi_s(x, y) \cdot \phi_z(z)$, which is substituted into the scalar Helmholtz equation to give the transverse- and z-wave equations. First, the z-wave equation is solved for the resonant frequency, and the resonant z-modal field is used to compute effective indices for the core and cladding regions These effective indices are in turn used in the transverse wave equation to compute the transverse wavenumber which is fed back to the z-wave equation. The two wave equations are solved alternately and iterated until convergence; which occurs typically in less than 10 seconds on a 350 MHz PC. The resonant frequencies and transverse field profile in the QW region agree very well with those of the Green's function method. However, the effective index method does not yield accurate threshold modal gain and photon lifetimes for oxide-confined VCSELs with very small aperture radius. For these parameters, pre-computed values from the Green's function method are used.

The electrical solver has been adopted from the version of Minilase developed for edge-emitting lasers [8], and it includes nonlinear gain, hot electron effects, spatial and spectral hole burning etc. To simulate the carrier transport in real space, Poisson's equation and continuity equation are solved for both electrons and holes by a Newton iteration. Drift-diffusion is assumed for carrier transport in the bulk regions as well as the lateral diffusion of QW carriers. At the heterojunctions that separate the bulk materials, the thermionic emission formula of Bethe [11] has been adopted:

$$j_{w\to b} = A^* T^2 \left[\exp\left(\frac{F_w - E_w - \Delta E}{k_B T} \right) - \exp\left(\frac{F_b - E_b}{k_B T} \right) \right] \quad (1)$$

where F_w/F_b and E_w/E_b are the quasi-Fermi level and the band edge in the well/barrier regions respectively, ΔE is the band edge discontinuity at the well/barrier interface, and $A^* = m^* k_B^2/(2\pi^2\hbar^3)$ is the Richardson constant. In the QW region, carriers are partitioned into continuum and bound states with separate quasi-Fermi levels. The carriers in the continuum states are ballistically coupled to carriers in the SCH regions, and by electron–phonon and electron–electron scatterings to carriers in the bound states. To account for hot carriers and spectral hole-burning effects, Minilase is also capable of simulating the QW carrier transport in the energy space by solving a one-dimensional Boltzmann-type equation based on detailed balance. In addition, an eight-band $k \cdot p$ method, which takes into account bandgap renormalisation and Coulomb enhancement effects, is self-consistently incorporated into Minilase to compute the bandstructure and optical matrix elements [12] as a function of position within the QW. A photon rate equation is solved to balance the global photon number of the fundamental mode. The variation of the local photon density is taken into account by calculating the transverse mode profile.

3 Simulation results and discussions

Minilase simulations are based on a double oxide-confined, 1-λ cavity VCSEL structure, which has experimentally shown a bandwidth greater than 16 GHz [2]. Since our major interest is in the intrinsic dynamics of the laser diode, we only simulate the active cavity for the electronic problem. The active cavity is the region between the top and the bottom oxide layers, excluding the upper and lower DBR regions. In the experiments, square apertures of $3 \times 3\ \mu m^2$ are used. In Minilase, cylindrical symmetry is assumed and the radius is set to be 1.8 μm unless otherwise specified. The schematic cross-section of the default device simulated in the electronic solver is shown in Fig. 1. The active region is a single 80 Å $In_{0.2}Ga_{0.8}As$ QW operating at 980 nm. The SCH regions can be either ungraded $Al_{0.1}Ga_{0.9}As$ or linearly graded from $Al_{0.1}Ga_{0.9}As$ to $Al_{0.6}Ga_{0.4}As$. The active region and the SCH are undoped. The oxide aperture is moderately doped at a density of $1 \times 10^{18}\ cm^{-3}$on both the p-side and n-side.

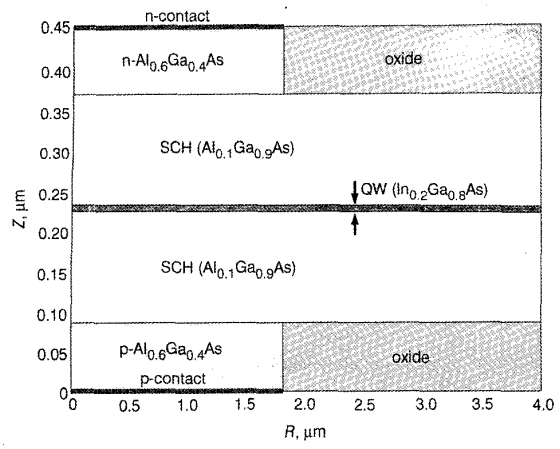

Fig. 1 *Schematic cross-section of a double oxide-confined, 1-λ cavity VCSEL structure simulated in the electrical solver of Minilase*

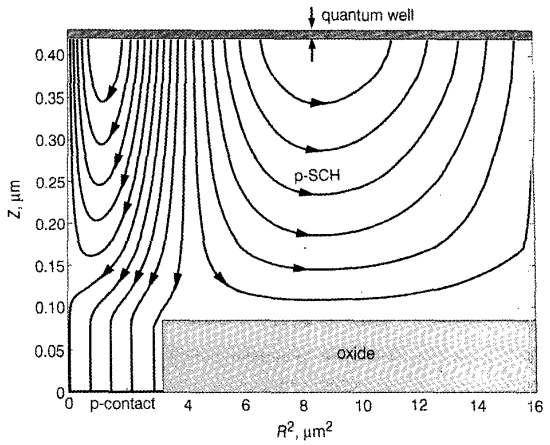

Fig. 2 *Contour plot of the simulated minority electron flux in p-SCH for an ungraded, 2-λ cavity VCSEL operating at 2 × I_{th}*
The square of the radius is used as the *x*-axis to correctly account for the cylindrical geometry of VCSELs

Throughout this paper, some variations of this structure are also simulated for comparison, and the difference will be highlighted for such cases. To obtain the modulation response in Minilase, a very small current step is applied to the steady-state bias and a time-dependent simulation is then performed [8].

3.1 Effect of minority carriers

The damping effects due to carrier transport across the QW have been studied based on rate equations [13, 14]. The rate equation models are usually not capable of solving the distributed carrier transport problem over the whole device. Previous Minilase simulations have revealed that a diffusion capacitance is induced by the wasted minority carriers for edge-emitting lasers [8]. Its damping effects on the modulation response is also shown [8] to be greatly reduced by doping the SCH regions. In this Section, the findings are extended to VCSEL structures and we examine the dependence of the diffusion capacitance on the thickness and grading profile of the SCH region. Graded 1-λ cavity designs are frequently used in experiments [2]. For the purpose of comparison, an artificial 2-λ cavity VCSEL, whose SCH thickness is approximately twice that of the 1-λ cavity structure, is also simulated. Graded and ungraded SCH regions are considered for both 1-λ and 2-λ cavity structures. To focus on the effects due to electronic transport, it is assumed that the resonant frequency, the optical confinement factor, the optical transverse mode pattern and the photon lifetime remain unchanged for all structures.

A contour plot of the simulated minority electron flux in the p-side region of an ungraded, 2-λ cavity device is shown in Fig. 2. It is observed that only a portion of the minority electrons can travel across the SCH region and reach the p-side contact. The rest of the minority electrons flow back into the QW. A fraction of them are reclaimed in the central region of the QW due to the strong SHB effect, i.e. the QW carrier density in the centre is much lower because of the strong stimulated recombination in that region, and therefore the minority electrons are attracted back into the well through thermionic emission. Some other minority electrons flow back to the outer region due to the barrier at the oxide layer. The spontaneous recombination of the minority carriers is insignificant since the typical carrier lifetime due to spontaneous emission is of the order of nanoseconds, which is much longer than the typical carrier transport time of ~100 ps. However, the dark recombination of minority carriers may be significant, particularly at the oxide interface. The accumulation of the minority carriers in the SCH region contributes to the so-called diffusion capacitance. Under direct modulation, higher frequency components of the AC current are more easily diverted through this diffusion capacitance [Note 1], and a severe roll-off is therefore induced in the modulation responses. This roll-off is clearly observed in the simulated responses for the ungraded, 2-λ cavity device, which are plotted as dashed lines in Fig. 3. As a comparison, the modulation responses of the same device with a linearly graded SCH region are simulated for the same values of bias (solid lines in Fig. 3). It can be seen that for the graded

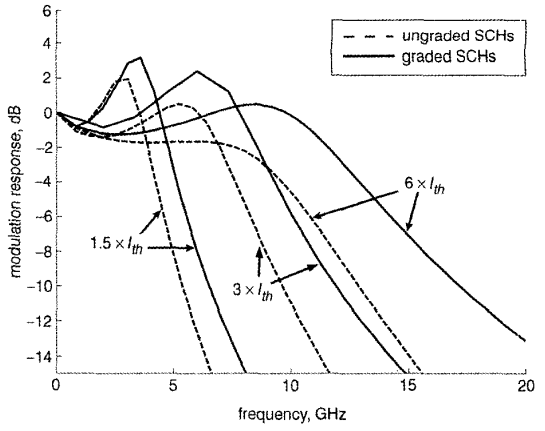

Fig. 3 *Simulated modulation responses for 2-λ cavity VCSELs with either ungraded or graded SCHs at three different biases*

Note 1: It is well known that, for a forward-biased p-n junction diode, the AC current passing through the diffusion capacitance has a frequency dependence of $\omega^{1/2}$ [15]. Our simulations show that the minority current in laser diodes has larger components at higher frequencies, too. However, the frequency dependence is more complicated than the simple power law of 1/2, because of the double heterostructure used in laser diodes and strong stimulated recombination in the QW.

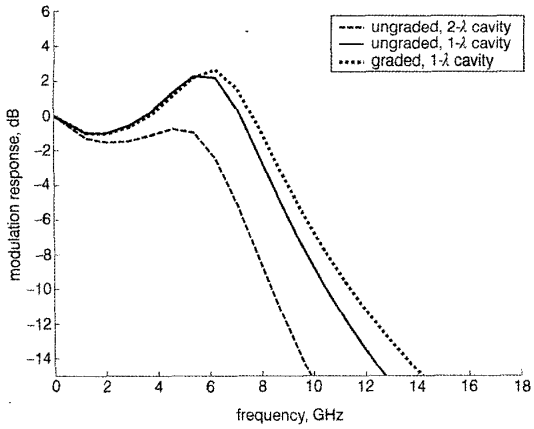

Fig. 4 *Simulated modulation responses at $3 \times I_{th}$ for ungraded 2-λ cavity, ungraded 1-λ cavity and graded 1-λ cavity*

structure, the roll-off is greatly reduced and hence, the modulation bandwidth is significantly increased. As a further example, the simulated modulation responses at a fixed bias of $3 \times I_{th}$ are plotted in Fig. 4 for three different structures: ungraded 2-λ cavity, ungraded 1-λ cavity, and graded 1-λ cavity. It is observed that for the shorter cavity VCSEL, the reduction of the roll-off is significant even with an ungraded SCH region, and grading the SCH region does not yield much further improvement. These observations indicate that the diffusion capacitance can be reduced by either grading the SCH region or reducing the cavity thickness. To further validate these deductions, Fig. 5 shows the distribution of the minority electrons plotted against the vertical direction (at $R = 0$) for an ungraded 2-λ cavity, an ungraded 1-λ cavity and a graded 2-λ cavity. The two curves corresponding to the ungraded structures have approximately the same peak density. However, the shorter SCH thickness of the 1-λ cavity device suppresses the total minority current more than the 2-λ cavity, and this results in a smaller diffusion capacitance for shorter cavity devices. For the graded 2-λ cavity, the density of minority electrons is about an order of magnitude smaller than the other two curves. A raised band edge caused by grading the cavity results in a very large suppression of minority carriers. The diffusion capacitance is hence highly suppressed in graded structures. Further simulations show that the rise of the SCH band edge of the ungraded, 2-λ cavity by increasing the Al composition leads to a similar suppression of the diffusion capacitance.

3.2 Effect of nonuniform transverse optical field

Due to strong index-guiding along the transverse direction in oxide-confined VCSELs, the transverse optical mode is tightly confined to a very small central region defined by the oxide aperture. As a result, the QW carriers in the central region are depleted much faster due to the stronger central stimulated recombination processes compared to those in the outer region. This represents the spatial hole-burning effect, which is believed to play an important role in the competition of multitransverse modes in the steady-state operations of VCSELs [16]. In this Section, it is demonstrated that the nonuniform transverse mode is also a key factor for defining the high-speed performance of single-mode, strongly index-guided VCSELs.

First the lateral diffusion due to the large gradient of carrier density caused by spatial hole burning is examined. Fig. 6 shows the simulated 2-D carrier density distribution inside the QW at two biases above threshold. As the bias increases, stronger carrier spatial hole-burning at the central region is clearly observed for both electrons and holes. It is also worthwhile to note in Fig. 6 that the local charge neutrality condition, assumed by most rate equation models under the approximation of ambipolar diffusion, is no longer valid inside the QW. The difference in electron and hole densities is due to differences in the transport properties of the two types of carriers [17]. In Fig. 7, the modulation responses are plotted for two cases, one with realistic carrier mobility in the QW, and the other with extremely low mobility. It can be seen that lateral diffusion of QW carriers does not reduce the modulation bandwidth by much, but dampens the relaxation oscillation peak slightly. In [7], the diffusion coefficient of QW carriers is varied within a reasonable range and little difference is observed in simulated modulation responses, which agrees with our simulation result.

Another more important nonlinear effect, particularly for small-aperture oxide-confined VCSELs, is directly associated with the nonuniform transverse optical field distribution. The stimulated recombination rate of QW carriers

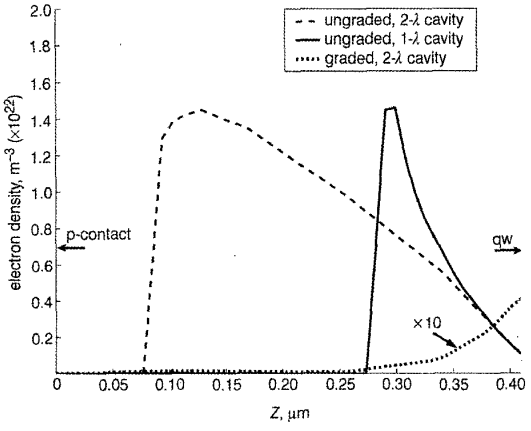

Fig. 5 *Simulated minority electron distribution along the vertical axis for ungraded 2-λ cavity, ungraded 1-λ cavity and graded 2-λ cavity*

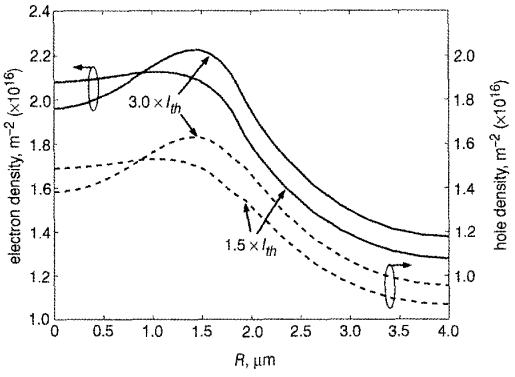

Fig. 6 *Simulated electron and hole density distribution along the radial direction of the QW*

Spatial hole-burning is observed as the current bias increases from $1.5 \times I_{th}$ to $3.0 \times I_{th}$

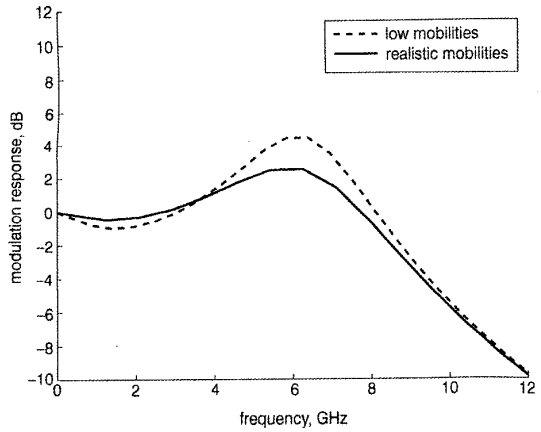

Fig. 7 *Simulated modulation responses at bias $2.5 \times I_{th}$ for ungraded, 1-λ cavity device*

The QW carrier mobilities are assigned either artificially low values ($\mu_{el} = \mu_{hl} = 10^{-6}$ m^2/V · s) or practical values ($\mu_{el} = 1.21$ and $\mu_{hl} = 0.04$ m^2/V · s)

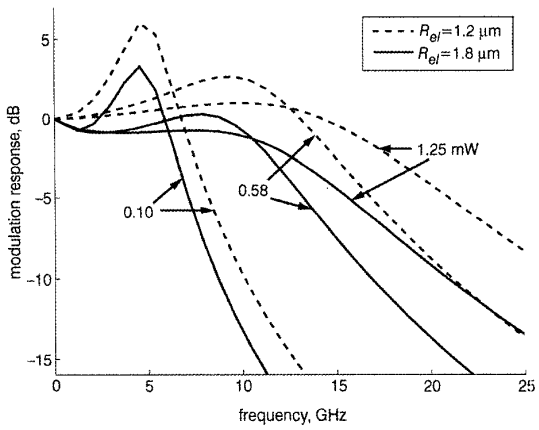

Fig. 8 *Simulated modulation responses for ungraded, 1-λ cavity device with the electrical aperture radius equal to 1.8 μm and 1.2 μm*

Optical aperture radius 1.8 μm in both structures. The responses are labelled according to their output power

is a function of position and can be expressed as $\tau_{st}^{-1} = v_g g' |E(r)|^2 S$, where v_g is the group velocity, g' is the differential material gain, S is the averaged photon density, and $|E(r)|^2$ is the normalised optical field such that $2\pi \int_{QW} |E(r)|^2 r\, dr = 1$. If we artificially divide the VCSEL laterally into many slices, and view each slice as an individual 'laser', then the relaxation frequency for each small 'laser' can be expressed as

$$\omega(r) = \sqrt{\frac{1}{\tau_{st}} \cdot \frac{1}{\tau_p}} = \sqrt{\frac{v_g g' |E(r)|^2 S}{\tau_p}} \qquad (2)$$

where τ_p is the photon lifetime. Since $|E(r)|^2$ is nonuniform within the transverse plane, ω_r varies with position, r. When the entire VCSEL is modulated at its relaxation frequency, Ω, those carriers at positions with $\omega(r) \neq \Omega$ are actually off-resonant. As a result, the total modulation response will be overdamped. In relation to (2) note that the differential material gain g' is nonuniform because it is a function of the carrier density and, as shown in Fig. 6, the carrier density varies within the QW plane. This nonuniformity also contributes to the variation of the local relaxation frequency and therefore the overdamping of the overall modulation response. However, this contribution is not significant in our case because the optical mode $|E(r)|^2$ changes far more drastically, while the nonlinearity in the material gain versus carrier density relation is quite moderate. Further simulations have been performed assuming a linear relation between the material gain and the carrier density, and strong overdamping in the response curve is still observed, which is due to the nonuniformity of the optical mode.

The gain suppression effect due to nonuniform photon density has previously been investigated for a two-section distributed feedback (DFB) laser [18]. Since the nonuniformity of the photon distribution is less severe in that case, and only low photon densities have been examined [18], this nonlinear effect was shown to be present, but not significant for the two-section DFB laser. However, for small-aperture oxide-confined VCSELs, the mode is tightly confined in a very small region and this nonlinear effect can have a large influence. To demonstrate this further, simulations of two devices, one with an electrical aperture size smaller than the optical aperture and the other with both electrical and optical sizes equal, were compared. In practice, a reduced electrical aperture can be achieved by using tapered oxide apertures [19]. The basic idea is to extend a thin oxidized 'finger' from the oxide layer toward the centre. As long as it is placed at a field null, the finger has little influence on the optical confinement, but reduces the area of current injection effectively. Fig. 8 shows the simulated modulated responses for both structures at biases corresponding to output power 0.10, 0.58 and 1.25 mW. For the device with reduced electrical aperture size, much reduced damping in the relaxation oscillation and significant increment in the modulation bandwidth are achieved. As demonstrated in a previous section, one cannot attribute such huge improvement to the reduction of the carrier lateral diffusion. In order to uncover the source of the improvement, the current density incident on the QW from the p-side and the optical transverse mode for both structures are plotted in Fig. 9. Both quantities are normalised with respect to their peak values. Since the same optical aperture radius (1.8 μm) is used, the transverse mode for both structures remains unchanged. As shown in Fig. 9, the optical mode intensity changes rapidly

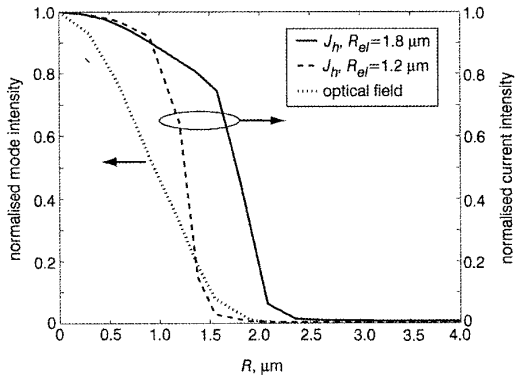

Fig. 9 *Normalised transverse optical intensity and current density incident from p-SCH onto the QW for ungraded, 1-λ cavity structure*

Electrical aperture radii of 1.8 μm and 1.2 μm were used. Optical aperture radius 1.8 μm in both cases

from its peak value at the centre to almost zero at the edge of the optical aperture at $R_{op} = 1.8\ \mu m$. On the other hand, the current distribution varies very slowly within the electrical aperture defined by R_{el}. For the device with both electrical and optical apertures equal, $R_{op} = R_{el} = 1.8\ \mu m$, a large fraction of the current is injected into the tail region of the optical mode profile. For the device with reduced electrical aperture ($R_{el} = 1.2\ \mu m$), the current injection is better confined in the region containing the peak optical density, and hence the damping effect due to the nonuniform photon density is significantly suppressed.

One concern with the reduced electrical aperture device is whether the confinement of current injection will cause additional lattice heating. As mentioned in the introduction, the thermal effects have not been included in the simulations presented in this paper. They may result in further reduction of the modulation bandwidth at high output power. To take these effects into account, a thermal diffusion equation also needs to be solved over the entire device and the detailed treatment is beyond the scope of this paper. Nevertheless, some preliminary simulation results have been obtained indicating that the additional temperature rise due to the tapered oxide aperture is less than 5K in the QW at the output power of 1.25 mW. This is because the reduced oxide aperture layer is very thin and the locally generated heat spreads out rapidly due to the thermal conduction of AlGaAs.

3.3 Comparison with experiment

A direct comparison can be made between the simulated modulation responses and those experimentally measured [2]. In the simulations, the following adjustments are made to match the device settings used in the experiment: the active region is composed of a 1-λ cavity with three 80 Å InGaAs quantum wells; the SCH region is graded; the resonant frequency is designed for 970 nm; and the aperture radius is set to 1.5 μm. Besides these data, we also have made some reasonable assumptions to account for missing experimental information. It has been indicated that the photon lifetime, τ_p, which is closely related to the threshold gain, is very sensitive to the thickness, the shape, the position, and the aperture size of the oxide layers due to diffraction and scattering losses [9, 20, 21]. The typical value for τ_p ranges from 1 ps to 6 ps for various structures as obtained from calculations with our optical solvers. Lacking the information of the actual composition of the oxide structure, $\tau_p = 2$ ps is assumed for this simulation.

Another assumption is related to the parasitic effects associated with the packaging and connecting leads to the device, as described in [8]. As previously mentioned, the electrical solver of Minilase only models the active cavity and currently does not include the resistance associated with the DBR stacks, the capacitance associated with the bond pads, and the inductance associated with the bond wires. Nonetheless, a 0.25 pF parallel capacitance is assumed to approximate the total of parasitic effects. The modulation response curves from these simulations and those from experiments [2] are plotted in Fig. 10 for three different values of output power. The experimental paper originally displays four curves, the last of which is multimode, and therefore no comparison is made with it. The figure shows good agreement in the relaxation frequency and −3 dB bandwidth for the first two bias values. At the highest output power, the computed relaxation frequency is still close to the experimental result, but there is a large error in the −3 dB bandwidth. This discrepancy is most likely due to hot electron and thermal effects, which are not included in the current simulations.

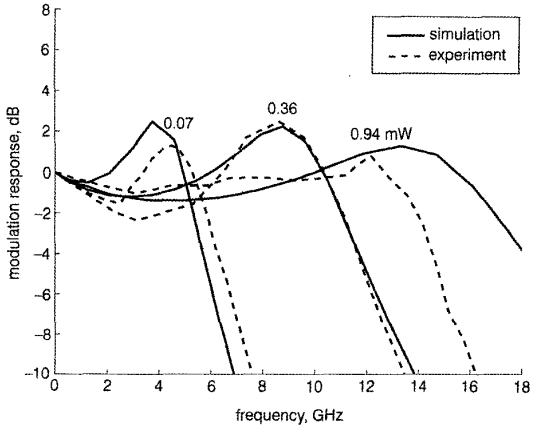

Fig. 10 *Measured [2] and simulated modulation responses for a 3-QW, 970 nm VCSEL*

Responses are labelled according to their output power. Simulation includes the effects of a 0.25 pF parasitic capacitance

4 Conclusions

The extension of Minilase to simulate the modulation response of VCSELs has demonstrated the importance of several carrier transport effects and their influence on the modulation response. Unlike rate equation approaches, Minilase is capable of modelling nonlinear gain effects based on physical principles and producing predictive results. Simulation results have been presented to demonstrate the effects of the real space carrier transport on the dynamic responses of VCSELs. It has been shown that a diffusion capacitance is induced by the minority carriers, which contributes to roll-offs in the response curves. Grading the SCH region or reducing the thickness of the cavity have been shown to be effective in reducing the diffusion capacitance and hence improving the modulation bandwidth. Another important overdamping effect has been found to be directly related to the nonuniform transverse optical field. Significant improvements in the modulation response can be achieved by reducing the electrical aperture size while keeping the optical aperture constant. Finally, comparisons of these simulations with experimental modulation response data show very good agreement at moderate output power.

5 Acknowledgments

This project has been supported by the Office of Naval Research (contract N0014-98-1-0604) and the National Science Foundation through the DesCArtES centre.

6 References

1 HUFFAKER, D.L., DEPPE, D.G., KUMAR, K., and ROGERS, T.J.: 'Native-oxide defined ring contact for low threshold vertical-cavity lasers', *Appl. Phys. Lett.*, 1994, **65**, pp. 97–99

2 LEAR, K.L., MAR, A., CHOQUETTE, K.D., KILCOYNE, S.P., SCHNEIDER, R.P., and GEIB, K.M.: 'High-frequency modulation of oxide-confined vertical cavity surface emitting lasers', *Electron. Lett.*, 1996, **32**, pp. 457–458

3 DEPPE, D.G., HUFFAKER, D.L., DENG, Q., and OH, T.-H.: 'Ultra-low threshold current vertical-cavity surface-emitting lasers for photonic integrated circuits', *IEICE Trans. Electron.*, 1997, **E80-C**, pp. 664–674

4 CHUANG, S.L.: 'Physics of optoelectronic devices' (Wiley, New York, 1995, 1st edn.)
5 COLDREN, L.A., and CORZINE, S.W.: 'Diode laser and photonic integrated circuits' (Wiley, New York, 1995, 1st edn.)
6 YU, S.F.: 'Dynamic behavior of vertical-cavity surface-emitting lasers', *IEEE J. Quantum Electron.*, 1996, **32**, pp. 1168–1179
7 YU, S.F., WONG, W.N., SHUM, P., and LI, E. Herbert: 'Theoretical analysis of modulation response and second-order harmonic distortion in vertical-cavity surface-emitting lasers', *IEEE J. Quantum Electron.*, 1996, **32**, pp. 2139–2147
8 GRUPEN, M., and HESS, K.: 'Simulation of carrier transport and nonlinearities in quantum well laser diodes', *IEEE J. Quantum Elcctron.*, 1998, **34**, pp. 120–140
9 OYAFUSO, F.A., KLEIN, B.D., REGISTER, L.F., and HESS, K.: 'Fully coupled electrical and optical simulation of VCSELs'. Proc. SPIE-Int. Soc. Opt. Eng., 2000, **3946**, pp. 108–116
10 KLEIN, B., REGISTER, L.F., HESS, K., DEPPE, D.G., and DENG, Q.: 'Self-consistent Green's function approach to the analysis of dielectrically apertured vertical-cavity surface-emitting lasers', *Appl. Phys. Lett.*, 1998, **73**, pp. 3324–3326
11 HESS, K.: 'Advanced theory of semiconductor devices' (Prentice Hall Press, Englewood Cliffs, New Jersey, 1988, 1st edn.)
12 OYAFUSO, F., VON ALLMEN, P., GRUPEN, M., and HESS, K.: 'Inclusion of bandstructure and many-body effects in a quantum well laser simulator', *VLSI Des.*, 1998, **8**, pp. 463–468
13 NAGARAJAN, R., ISHIKAWA, M., FUKUSHIMA, T., GEELS, R.S., and BOWERS, J.E.: 'High speed quantum-well lasers and carrier transport effects', *IEEE J. Quantum Electron.*, 1992, **28**, pp. 1990–2007
14 RIDEOUT, W., SHARFIN, W.F., KOTELES, E.S., VASSELL, M.O., and ELMAN, B.: 'Well-barrier hole burnings in quantum well lasers', *IEEE Photonics Technol. Lett.*, 1991, **3**, pp. 784–786
15 SZE, S.M.: 'Physics of semiconductor devices' (Wiley, New York, 1981, 2nd edn.)
16 VALLE, A., SARMA, J., and SHORE, K.A.: 'Spatial holeburning effects on the dynamics of vertical cavity surface-emitting laser diodes', *IEEE J. Quantum Electron.*, 1995, **31**, pp. 1423–1431
17 KOSINOVSKY, G.A., GRUPEN, M., and HESS, K.: 'Effect of carrier charge imbalance on the threshold current in diode lasers with thin intrinsic quantum wells', *Appl. Phys. Lett.*, 1994, **65**, pp. 3218–3220
18 FENG, J., CHEN, T.R., and YARIV, A.: 'Effects of non-uniform photon distribution on high speed response in semiconductor distributed feedback lasers', *Appl. Phys. Lett.*, 1995, **67**, pp. 3706–3708
19 HEGBLOM, E.R., MARGALIT, N.M., FIORE, A., and COLDREN, L.A.: 'High-performance small vertical-cavity lasers: a comparison of measured improvements in optical and current confinement in devices using tapered apertures', *IEEE J. Sel. Top. Quantum Electron.*, 1999, **5**, pp. 553–560
20 HEGBLOM, E.R., BABIC, D.I., THIBEAULT, B.J., and COLDREN, L.A.: 'Scattering losses from dielectric apertures in vertical-cavity lasers', *IEEE J. Sel. Top. Quantum Electron.*, 1997, **3**, pp. 379–389
21 BOND, A.E., DAPKUS, P.D., and O'BREIN, J.D.: 'Aperture placement effects in oxide-defined vertical-cavity surface-emitting lasers', *IEEE Photonics Technol. Lett.*, 1998, **10**, pp. 1362–1364